

SUPPORTING INFORMATION

Size-Dependent Catalytic Kinetics and Dynamics of Pd nanocubes: a Single-Particle Study

Tao Chen^{a,b}, Yuwei Zhang^a, Weilin Xu^{a*}

^aState Key Laboratory of Electroanalytical Chemistry, & Jilin Province Key Laboratory of Low Carbon Chemical Power, Changchun Institute of Applied Chemistry, Chinese Academy of Science, 5625 Renmin Street, Changchun 130022, P.R. China.

^bGraduate University of Chinese Academy of Science, Beijing, 100049, China.

*To whom correspondence. Email: weilinxu@ciac.ac.cn (W. X.)

1. Experimental Methods

1.1 Chemicals and synthesis Methods

Poly(vinyl pyrrolidone) (PVP, MW \approx 55 000), sodium tetrachloropalladate(II) (Na_2PdCl_4), PdCl_2 were purchased from Alfa Aesar, PVP (MW \approx 30 000, K-30), formamide (FA), L-ascorbic acid (AA), potassium iodide (KI), potassium bromide (KBr), potassium chloride (KCl), formaldehyde solution (HCHO, 37 wt% in H_2O) were purchased from Sinopharm Chemical Reagent Co. Ltd. (Shanghai, China). All chemical reagents were used as received without further purification. Ultrapure Millipore water ($18.2 \text{ M}\Omega\cdot\text{cm}$) was used as the solvent throughout. All the vials were made from borosilicate glass, with a black phenolic molded screw cap and polyvinyl-faced pulp liner.

Synthesis of 5.2 nm Pd nanocubes. 5.0 mL of formamide solution containing PVP (K-30, 50 mg) and KI (17 mg) were placed in a 20 mL vial, and pre-heated in air under magnetic stirring at 120°C for 10 min. PdCl_2 powder (36 mg) was added and maintained at 120°C for 60 min. The product was collected by centrifugation and washed 10 times with water to remove excess PVP.

Synthesis of 7.0 nm Pd nanocubes. 8.0 mL of an aqueous solution containing PVP (MW \approx 55 000 mg), AA (60 mg), KBr (5 mg) and KCl (185 mg) were placed in a 20 mL vial, and pre-heated in air under magnetic stirring at 80°C for 10 min. Then, 3.0 mL of an aqueous solution containing Na_2PdCl_4 (57 mg) was added using a pipette. After the vial had been capped, the reaction was allowed to proceed at 80°C for 3 h. The product was collected by centrifugation and washed 10 times with water to remove excess PVP.

Synthesis of 11.4 nm Pd nanocubes. 8.0 mL of an aqueous solution containing PVP (MW \approx 55 000 mg), AA (60 mg), and KBr (300 mg) were placed in a 20 mL vial, and

pre-heated in air under magnetic stirring at 80°C for 10 min. Then, 3.0 mL of an aqueous solution containing Na₂PdCl₄ (57 mg) was added using a pipette. After the vial had been capped, the reaction was allowed to proceed at 80°C for 3 h. The product was collected by centrifugation and washed 10 times with water to remove excess PVP.

Synthesis of 15.2 nm Pd nanocubes. 8.0 mL of an aqueous solution containing PVP (MW ≈ 55 000 mg), AA (60 mg), KBr (600 mg) were placed in a 20 mL vial, and pre-heated in air under magnetic stirring at 80°C for 10 min. Then, 3.0 mL of an aqueous solution containing Na₂PdCl₄ (57 mg) was added using a pipette. After the vial had been capped, the reaction was allowed to proceed at 80°C for 3 h. The product was collected by centrifugation and washed 10 times with water to remove excess PVP.

Synthesis of 22.2 nm Pd nanocubes. 2.5 mL of aqueous Na₂PdCl₄ solution (19 mg/mL) was introduced into 8 mL of an aqueous solution containing PVP (105 mg), HCHO (100 μL), and 0.3 mL of an aqueous suspension (1.8 mg mL⁻¹ in concentration) of Pd cubic seeds 11.4 nm in edge length, which had been heated at 60°C for 5 min under magnetic stirring in a capped vial. The reaction was allowed to proceed at 60°C for 3 h. The product was collected by centrifugation and washed 10 times with water to remove excess PVP.

1.2 Size distributions and shape distributions of Pd nanocubes.

The prepared Pd nanocubes all have well-defined facets, which can be seen in the SEM images (Figure S1 and Figure 1). In the X-ray diffraction (XRD) patterns recorded on 5.2 nm Pd nanocubes, five peaks were observed for each pattern which can be indexed to the (111), (200), (220), (311), and (222) reflections of a face-centered cubic (fcc) structure of metallic Pd (JCPDS, card no. 05-0681), showing the crystalline nature of the prepared particles (Figure S1c). In the X-ray photoelectron spectroscopy (XPS), two peaks located at 340.7 and 335.3 eV can be assigned to elemental Pd 3d_{3/2} and Pd 3d_{5/2}, respectively. The shoulders at higher energies (342.2 eV for Pd 3d_{3/2} and 338.0 eV for Pd 3d_{5/2}) can be assigned to Pd (II) samples (Figure S1 d). The Pd (II) contents occupied about 15% of the whole surface area for all these five sets of Pd nanocubes. For example, Fig. S1d shows the typical results for both 5.2 nm and 22.2 nm Pd cubes from the XPS analysis. Although the Pd (II) component existed here, it does not affect our result due to the same coverage rate of Pd (II) on different size Pd cubes..

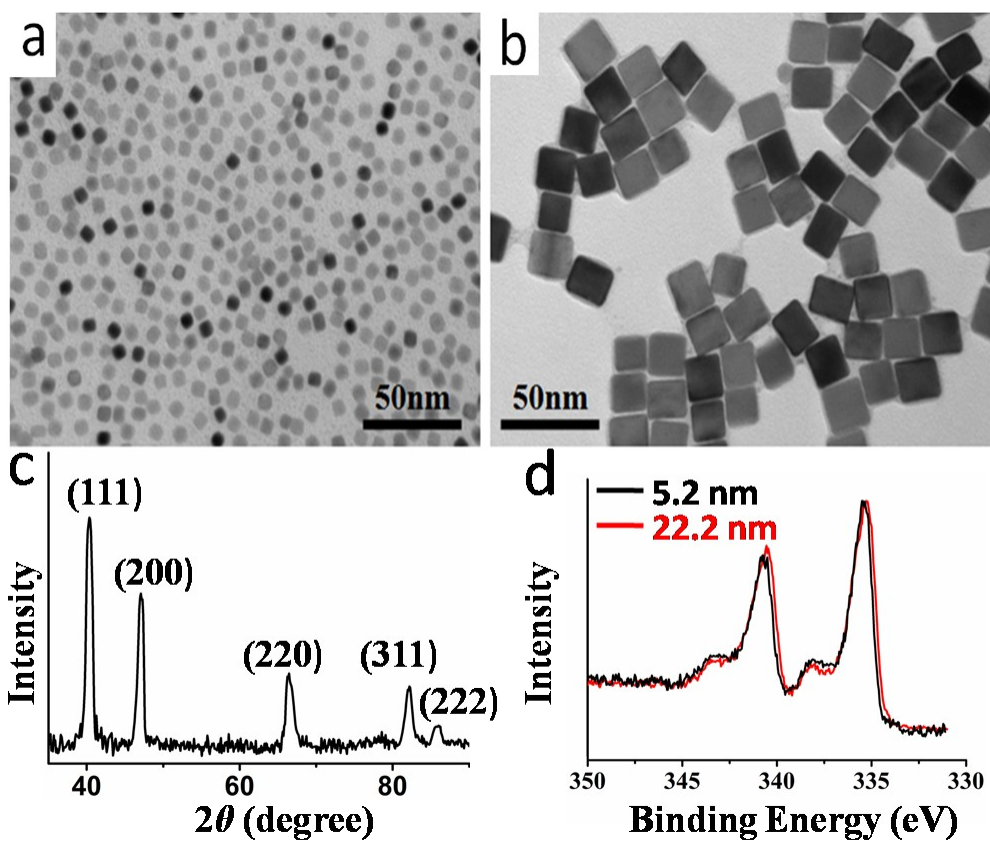


Figure S1. Typical TEM images of two sets of Pd nanocubes with sizes (a) 5.2 nm, (b) 22.2 nm. (c) XRD characterization of 5.2 nm Pd nanocubes. (d) XPS characterization of 5.2 nm and 22.2 nm Pd nanocubes.

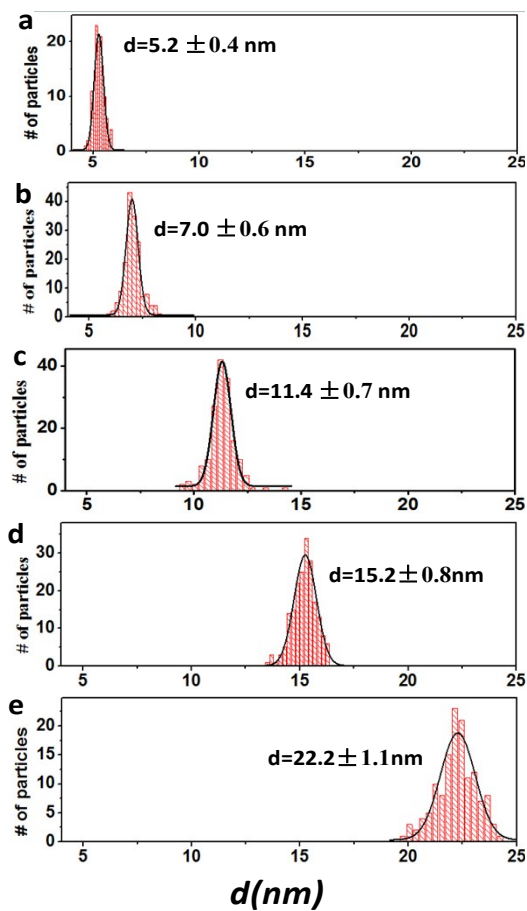


Figure S2. Size distributions of five sets size-different Pd nanocrystals used in this study. (a) 5.2 nm, (b) 7.0 nm, (c) 11.4 nm, (d) 15.2 nm, (e) 22.2 nm.

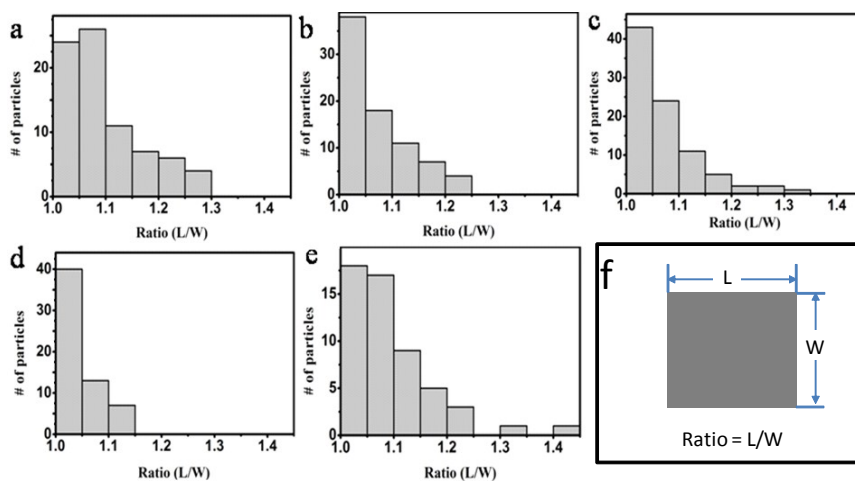


Figure S3. Shape distributions of five sets size-different Pd nanocrystals. (a) 5.2 nm, (b) 7.0 nm, (c) 11.4 nm, (d) 15.2 nm, (e) 22.2 nm. (f) Scheme to show how the ratio is calculated. L/W means the ratio of a nanocube's length (L) and width (W), and $L \geq W$. All samples show narrow shape-distribution.

1.3 Ensemble measurements of Pd nanocubes catalyzed reaction

We tested the ability of the Pd nanocubes in catalyzing the reduction of resazurin to resorufin by hydrogen in ensemble measurements. The control experiments show there is no reduction reaction between resazurin and hydrogen without Pd nanocatalysts, and there is no reaction between resazurin and Pd nanocubes without hydrogen. After the addition of Pd nanocubes to the reaction solution containing both resazurin (Molecular Probes, Invitrogen) and hydrogen, the catalytic reaction proceeds and was monitored by UV-Vis absorption. The experiment was carried out in water at room temperature. We test all three sets of Pd nanocubes with different size. The color of solution turns from blue (resazurin) to red (resorufin) gradually upon the injection of Pd nanocubes. The absorption spectrum of the reaction shows a decrease of the resazurin absorption at 598 nm over time and an increase of the resorufin at 568 nm (Figure S4). The plasmon band of the Pd nanocubes is not observable due to the super-low concentration of Pd nanocubes (6 fM). The isobestic point in the absorption spectra clearly indicates the quantitative conversion of resazurin to resorufin catalyzed by Pd nanocubes. The time profiles of the absorbance at 568 nm and 598 nm show the quantitative conversion of resazurin to resorufin catalyzed by Pd nanocubes (Figure S4 b, d, f). The rate of resazurin reduction reaction increases with the increase of size of Pd nanocubes (Figure S4 g,h): with the same concentration of resazurin and Pd nanocubes, the small-sized Pd nanocubes accomplish the reaction with longer time than the size-larger ones.

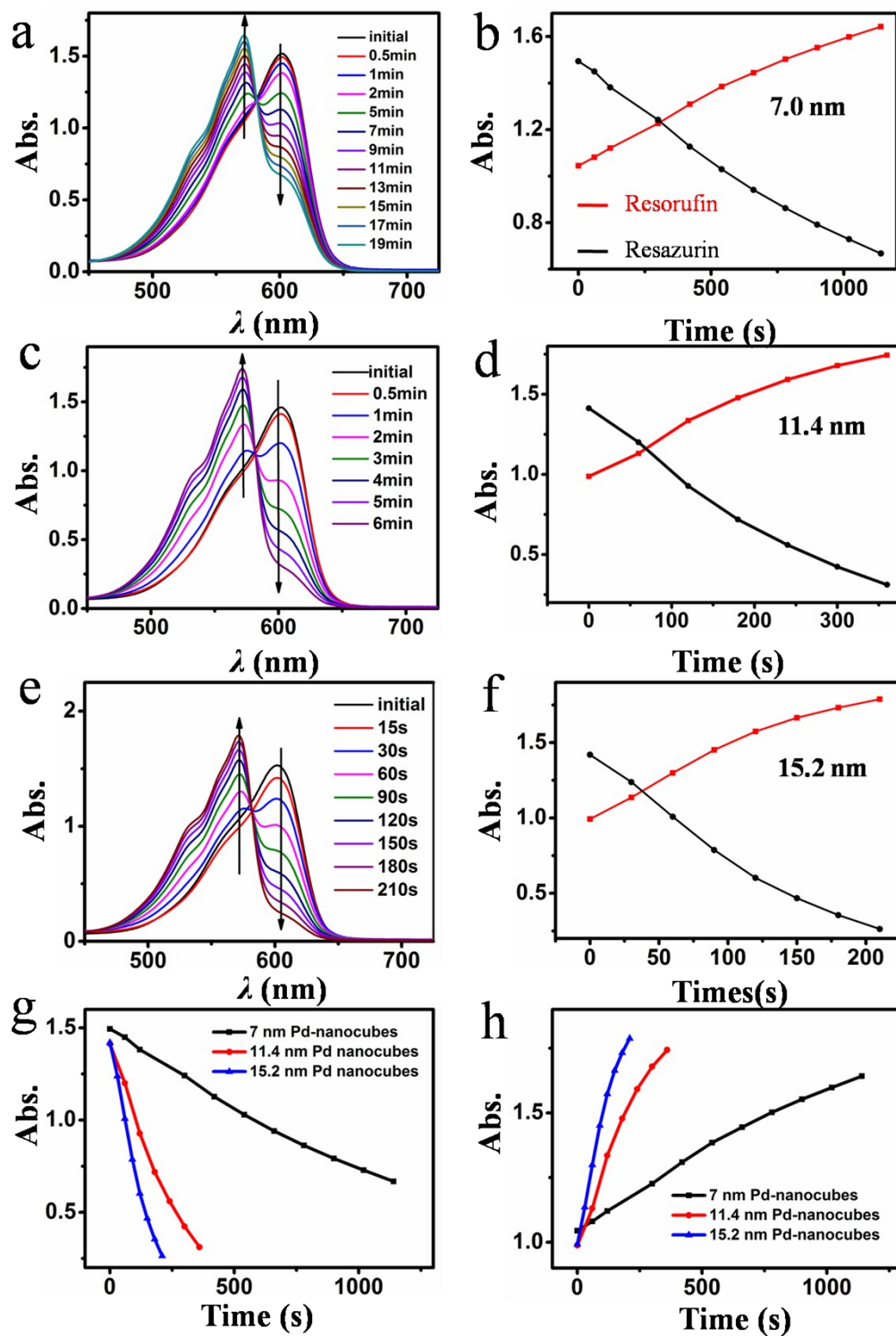


Figure S4. In situ absorption measurements of resazurin reduction by H₂ catalyzed by (a) 7 nm Pd nanocubes (c) 11.4 nm Pd nanocubes (e) 15.2 nm Pd nanocubes in aqueous solution. [resazurin]₀ = 33 μ M. [Pd nanocubes]₀ = 6 fM. (b) (d) (f) are the time profiles of absorbance at 568 nm (resorufin) and 598 nm (resazurin) from (a), (c), (e), respectively. (g,h) Time profiles of absorbance at 598 (g) and 568 (h) nm from (a) (c) (e).

2. Control experiments on possible effects of flow rate, Br⁻ and PVP on catalysis.

The flow rate (10 uL/min) in the microfluidic cell we used here is same as previous report¹. Many studies carried on the experiments at the flow rate between 5 uL/min and 15 uL/min¹⁻³. To see the flow rate dependence of $\langle\tau_{\text{off}}\rangle^{-1}$ and $\langle\tau_{\text{on}}\rangle^{-1}$, we carried the single-molecule experiment using 15.2 nm Pd nanocubes as representative at different flow rate with fixed concentration of resazurin and hydrogen (Figure S5 a,b). No flow rate dependence could be observed in the range from 5 uL/min to 20 uL/min on both $\langle\tau_{\text{off}}\rangle^{-1}$ and $\langle\tau_{\text{on}}\rangle^{-1}$.

Different amounts of Br⁻ and PVP are added to generate size different Pd nanocubes as stabilization ligands. Although these nanoparticles were extensively washed with water (10 times) after the synthesis as shown above and then thoroughly washed after immobilization on the quartz surface, residual Br⁻ and PVP may still preset and play roles in the catalysis both in the product formation reaction and product desorption reaction. To probe the possible effect of Br⁻ and PVP on catalysis, we studied the Pd-nanoparticle catalysis in the presence of Br⁻ and PVP at the single-molecule level using 15.2 nm Pd nanocubes as representative. At fixed [resazurin] and [H₂], $\langle\tau_{\text{off}}\rangle^{-1}$ and $\langle\tau_{\text{on}}\rangle^{-1}$, as shown in the following Figure S7, the single-particle rates of product formation and desorption, show no dependence on the Br⁻ concentration up to 500 nM and the PVP concentration up to 500 ng/mL. The two concentrations are all many times larger than the residual Br⁻ and PVP on Pd nanocube surface (Figure S5 c,d,e,f). This fact indicates that the possible effect of residual Br⁻ and PVP on nanocatalysis could be neglected under our experimental conditions.

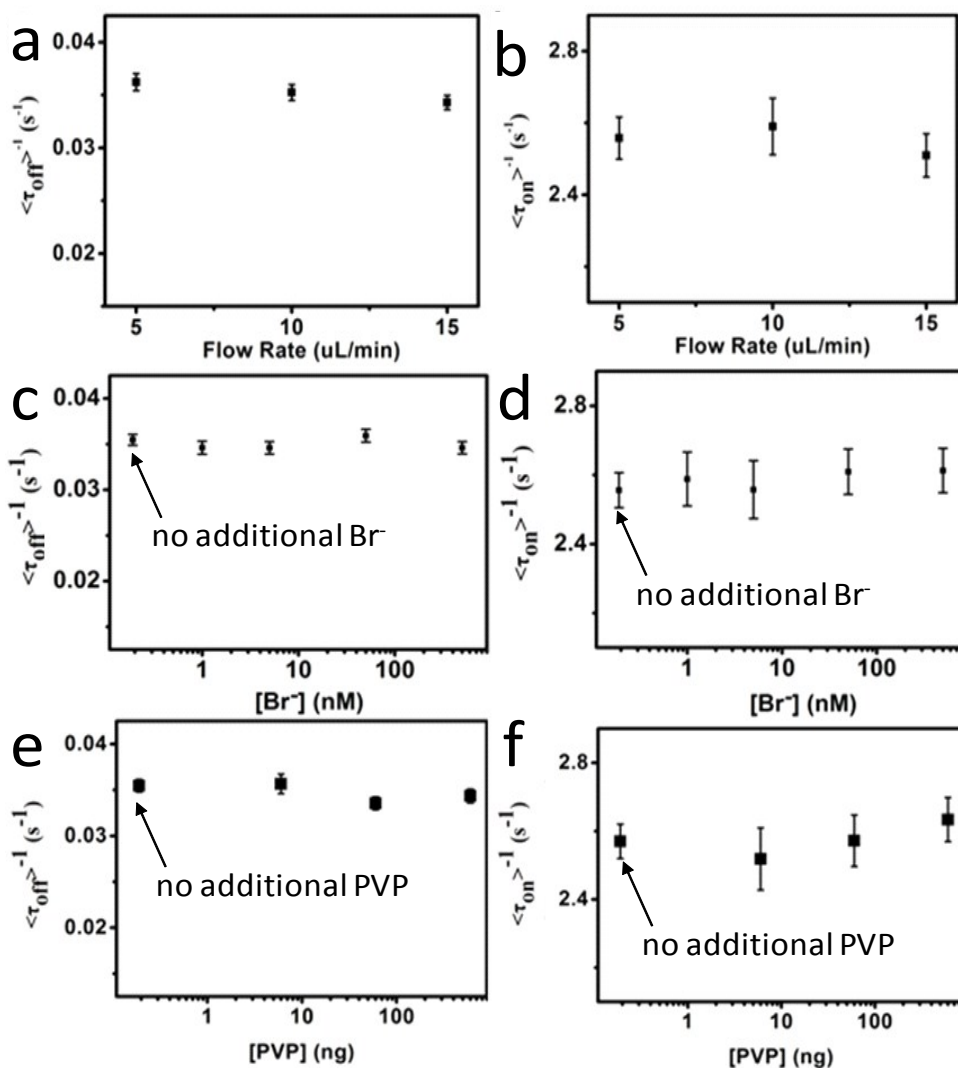
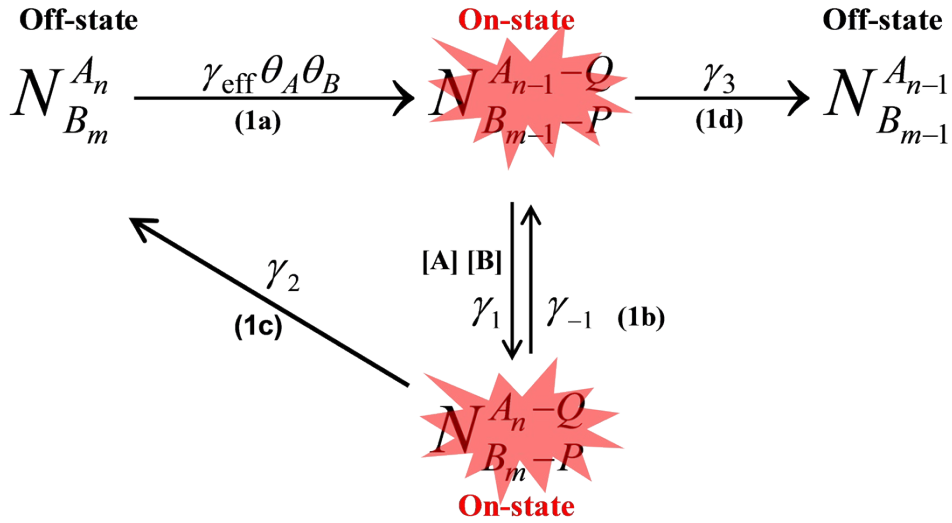


Figure S5. Flow rate dependence of (a) $\langle\tau_{\text{off}}\rangle^{-1}$ and (b) $\langle\tau_{\text{on}}\rangle^{-1}$. Titration of (c) $\langle\tau_{\text{off}}\rangle^{-1}$ and (d) $\langle\tau_{\text{on}}\rangle^{-1}$ with increasing Br^- concentration and titration of (e) $\langle\tau_{\text{off}}\rangle^{-1}$ and (f) $\langle\tau_{\text{on}}\rangle^{-1}$ with increasing PVP concentration. The experiments were carried on 15.2 nm Pd nanoparticles; each data point is averaged over more than 80 nanoparticles; The hydrogen concentration was fixed at 0.8 mM and $[\text{resazurin}] = 1 \text{ nM}$. Error bar was s.e.m..

The above three control experiments are done to exclude the possible effect of flow rate, residual Br^- and PVP on the observed single-molecule signal, such as $\langle\tau_{\text{off}}\rangle^{-1}$ and $\langle\tau_{\text{on}}\rangle^{-1}$.

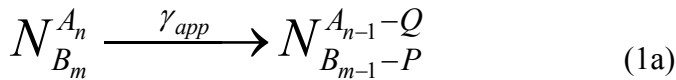
3. Derivation of single-molecule kinetic equations.



Scheme S1: The kinetic mechanism for a catalytic redox reaction by Pd nanocubes.

3.1 Derivation of the distribution of the off-time, $f_{\text{off}}(\tau)$, and of $\langle \tau_{\text{off}} \rangle^{-1}$.

The mechanism assumes that the two kinds of substrate molecules bind to the Pd nanocubes surfaces reversibly at a fast adsorption equilibrium all the time². The surface coverage of substrate molecule on one nanoparticle is governed by the Langmuir adsorption isotherm⁴. According to this mechanism, the reaction of the two kinds of molecules that takes place during the off-times of a single-turnover trajectory of fluorogenic reactions is reaction 1a in Scheme 1:



where A,B represent hydrogen and resazurin, respectively; n , m is the number of H_2 and substrate molecular adsorbed on the nanoparticle surface at equilibrium; γ_{app} is the apparent rate constant for forming one product of one nanoparticle and takes the form

$$\gamma_{app} = \gamma n_A n_B = \gamma n_T^2 \theta_A \theta_B \quad (S1)$$

Where γ is the rate constant representing the intrinsic reactivity per catalytic site for the catalytic conversion reaction; n_A and n_B are the numbers of A and B molecule adsorbed on at the catalytic site; n_T is the total number of the surface catalytic sites on one nanoparticle; θ_A , θ_B is the fraction of the occupied surface catalytic sites by H_2 and substrate. Form the Langmuir adsorption isotherm:

$$n_A = n_T \theta_A = n_T \frac{a_A [A]}{1 + a_A [A] + a_B [B]} \quad (S2)$$

$$n_B = n_T \theta_B = n_T \frac{a_B [B]}{1 + a_A [A] + a_B [B]} \quad (\text{S3})$$

Here a_A, a_B is the H_2 and substrate binding and unbinding rate constants, then we get

$$\gamma_{app} = \gamma n_T^2 \frac{a_A [A] a_B [B]}{(1 + a_A [A] + a_B [B])^2} \quad (\text{S4})$$

In conventional ensemble measurements where the catalysis by a large of nanoparticles is measures in solution , the kinetic rate equations is

$$\frac{d[N_{B_{m-1}-P}^{A_{n-1}-Q}]}{dt} = -\frac{d[N_{B_m}^{A_n}]}{dt} = \gamma_{app} [N_{B_m}^{A_n}] \quad (\text{S5})$$

Where $[N_{B_m}^{A_n}]$ is the concentration of nanoparticles that do not carry any product, and $[N_{B_{m-1}-P}^{A_{n-1}-Q}]$ is the concentration of nanoparticles on which one product molecule is generated.

Under the condition of single-nanoparticle measurements, the concentration of one nanoparticle is meaningless and needs to be replaced by the probability of the single nanoparticle. Then we have

$$\frac{dP_{N_{B_{m-1}-P}^{A_{n-1}-Q}}(t)}{dt} = -\frac{dP_{N_{B_m}^{A_n}}(t)}{dt} = \gamma_{app} P_{N_{B_m}^{A_n}}(t) \quad (\text{S6})$$

Where $P(t)$ is the probabilities for finding the single nanoparticle in the state $N_{B_{m-1}-P}^{A_{n-1}-Q}$ and

$N_{B_m}^{A_n}$. At the onset of each τ_{off} reaction ($t=0$), no product molecule has formed. So the initial conditions for the equation are $P_{N_{B_{m-1}-P}^{A_{n-1}-Q}}(t)=0$, $P_{N_{B_m}^{A_n}}(t)=1$.

And at any time within τ_{off} , $P_{N_{B_{m-1}-P}^{A_{n-1}-Q}}(t) + P_{N_{B_m}^{A_n}}(t) = 1$

We can then evaluate the probability density of the time $\Delta\tau$ needed to complete the off-time reaction, $f_{\text{off}}(\tau)$, that is, the probability density is τ_{off} . The probability for finding a particle τ is $f_{\text{off}}(\tau)\Delta\tau$, which is equal to the probability of switching from the

$N_{B_m}^{A_n}$ state to the $N_{B_{m-1}-P}^{A_{n-1}-Q}$ state for the nanoparticle between $t = \tau$ and $t = \tau + \Delta\tau$. In the limit of infinitesimal $\Delta\tau$, we obtain:

$$f_{off}(\tau) = \frac{dP_{N_{B_{m-1}-P}^{A_{n-1}-Q}}(t)}{dt} = \gamma_{app} P_{N_{B_m}^{A_n}}(t) = \gamma n_T^2 \frac{a_A [A] a_B [B]}{(1 + a_A [A] + a_B [B])^2} P_{N_{B_m}^{A_n}}(t) \quad (S7)$$

Solving Equations 6 for $P_{N_{B_m}^{A_n}}(t)$ with the initial conditions, we have:

$$f_{off}(\tau) = \gamma n_T^2 \frac{a_A [A] a_B [B]}{(1 + a_A [A] + a_B [B])^2} \exp\left(-\gamma n_T^2 \frac{a_A [A] a_B [B]}{(1 + a_A [A] + a_B [B])^2} \tau\right) = \gamma_{app} \exp(-\gamma_{app} \tau) \quad (S8)$$

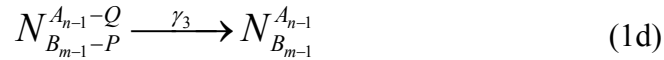
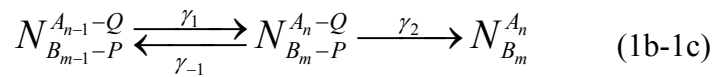
Then, $\langle \tau_{off} \rangle^{-1}$ represents the rate of product formation for a single nanoparticle :

$$\langle \tau_{off} \rangle^{-1} = \frac{1}{\int_0^\infty \tau f_{off}(\tau) d\tau} = \gamma n_T^2 \frac{a_A [A] a_B [B]}{(1 + a_A [A] + a_B [B])^2} = \frac{\gamma_{eff} a_A [A] a_B [B]}{(1 + a_A [A] + a_B [B])^2} \quad (S9)$$

Where, $\gamma_{eff} = \gamma n_T^2$. In our experiments, the concentration of H_2 is fixed and the $[A]$ can be seen as a constant. Form this equation, $\langle \tau_{off} \rangle^{-1}$ should increase initial and then decrease with increasing substrate concentration $[B]$.

3.2 Derivation of the distribution of the on-time, f_{on} , and of $\langle \tau_{on} \rangle^{-1}$.

For product desorption, we considered two parallel desorption reaction pathways: one a substrate-assisted pathway (1b-1c) and the other a direct desorption pathway (1d):



Under the assumptions of the mechanism where fast substrate adsorption equilibrium is established at all time, $N_{B_{m-1}}^{A_{n-1}}$ state will be quickly turned to the $N_{B_m}^{A_n}$ state, as substrate molecular in the solution will quickly bind to an available site to maintain the equilibrium. The conventional kinetic rate equations in concentration terms:

$$\frac{d[N_{B_{m-1}-P}^{A_{n-1}-Q}]}{dt} = -(\gamma_1 [A][B] + \gamma_3) [N_{B_{m-1}-P}^{A_{n-1}-Q}] + \gamma_{-1} [N_{B_m-P}^{A_n-Q}] \quad (S10)$$

$$\frac{d[N_{B_m-P}^{A_n-Q}]}{dt} = \gamma_1 [A][B][N_{B_{m-1}-P}^{A_{n-1}-Q}] - (\gamma_{-1} + \gamma_2)[N_{B_m-P}^{A_n-Q}] \quad (\text{S11})$$

$$\frac{d[N_{B_m}^{A_n}]}{dt} = \gamma_2 [N_{B_m-P}^{A_n-Q}] \quad (\text{S12})$$

$$\frac{d[N_{B_{m-1}}^{A_{n-1}}]}{dt} = \gamma_3 [N_{B_{m-1}-P}^{A_{n-1}-Q}] \quad (\text{S13})$$

In single-molecule measurements, the concentration terms of nanoparticles was replaced with their probabilities. We obtained:

$$\frac{dP_{N_{B_{m-1}-P}^{A_{n-1}-Q}}(\tau)}{d\tau} = -(\gamma_1 [A][B] + \gamma_3) P_{N_{B_{m-1}-P}^{A_{n-1}-Q}}(\tau) + \gamma_{-1} P_{N_{B_m-P}^{A_n-Q}}(\tau) \quad (\text{S14})$$

$$\frac{dP_{N_{B_m-P}^{A_n-Q}}(\tau)}{d\tau} = \gamma_1 [A][B] P_{N_{B_{m-1}-P}^{A_{n-1}-Q}}(\tau) - (\gamma_{-1} + \gamma_2) P_{N_{B_m-P}^{A_n-Q}}(\tau) \quad (\text{S15})$$

$$\frac{dP_{N_{B_m}^{A_n}}(\tau)}{d\tau} = \gamma_2 P_{N_{B_m-P}^{A_n-Q}}(\tau) \quad (\text{S16})$$

$$\frac{dP_{N_{B_{m-1}}^{A_{n-1}}}(\tau)}{d\tau} = \gamma_3 P_{N_{B_{m-1}-P}^{A_{n-1}-Q}}(\tau) \quad (\text{S17})$$

The initial conditions for solving the Equations S14-S17 are $P_{N_{B_{m-1}-P}^{A_{n-1}-Q}}(\tau)=0$,

$P_{N_{B_m-P}^{A_n-Q}}(\tau)=0$, $P_{N_{B_m}^{A_n}}(\tau)=0$, $P_{N_{B_{m-1}-P}^{A_{n-1}-Q}}(\tau)=0$ with $t = 0$ being the onset of each on-time τ_{on} ,

and at any time within τ_{on} , and

$$P_{N_{B_{m-1}-P}^{A_{n-1}-Q}}(\tau) + P_{N_{B_m-P}^{A_n-Q}}(\tau) + P_{N_{B_m}^{A_n}}(\tau) + P_{N_{B_{m-1}-P}^{A_{n-1}-Q}}(\tau) = 1.$$

We can then consider the probability density $f_{\text{on}}(\tau)$ of the on-time τ_{on} . τ_{on} is the time required to finish reactions in eq 1c or the reaction eq 1d. The probability of finding a particular τ is $f_{\text{on}}(\tau)\Delta\tau$, which is equal to the sum of the probability for the nanoparticle to switch from the $N_{B_m-P}^{A_n-Q}$ states to the $N_{B_m}^{A_n}$ state between τ and $\tau + \Delta\tau$ and the probability for the nanoparticle to switch from the $N_{B_{m-1}-P}^{A_{n-1}-Q}$ state to the $N_{B_{m-1}}^{A_{n-1}}$ state between τ and $\tau + \Delta\tau$. In the limit of infinitesimal $\Delta\tau$, we have

$$f_{on}(\tau) = \frac{dP_{N_{B_{m-1}}^{A_{n-1}}}(\tau)}{d\tau} + \frac{dP_{N_{B_m}^{A_n}}(\tau)}{d\tau} = \gamma_3 P_{N_{B_{m-1}-P}^{A_{n-1}-Q}}(\tau) + \gamma_2 P_{N_{B_m-P}^{A_n-Q}}(\tau) \quad (S18)$$

Solving eqs (S14-S17) for $P_{N_{B_{m-1}-P}^{A_{n-1}-Q}}(\tau)$ and $\gamma_3 P_{N_{B_m-P}^{A_n-Q}}(\tau)$ using the initial conditions, we get

$$f_{on}(\tau) = \frac{1}{2\alpha} \left[M e^{(\alpha+\beta)\tau} + N e^{(\beta-\alpha)\tau} \right] \quad (S19)$$

$$\alpha = \sqrt{(\gamma_1 [A][B] + \gamma_{-1} + \gamma_2 + \gamma_3)^2 / 4 - (\gamma_1 \gamma_2 [A][B] + \gamma_{-1} \gamma_3 + \gamma_2 \gamma_3)}$$

$$\beta = -(\gamma_1 [A][B] + \gamma_{-1} + \gamma_2 + \gamma_3) / 2$$

$$M = \gamma_1 \gamma_2 [A][B] + \gamma_3 \alpha + \gamma_3 \beta + \gamma_{-1} \gamma_3 + \gamma_2 \gamma_3$$

$$N = -\gamma_1 \gamma_2 [A][B] + \gamma_3 \alpha - \gamma_3 \beta - \gamma_{-1} \gamma_3 - \gamma_2 \gamma_3$$

Depending on the substrate concentration and the magnitudes of the individual rate constants, $f_{on}(\tau)$ will exhibit different shapes⁵. If complete shutdown of the substrate-assisted desorption pathway, that is, $\gamma_1 = \gamma_{-1} = \gamma_2 = 0$. Equation S19 the reduces to $f_{on}(\tau)_{\gamma_1 = \gamma_{-1} = \gamma_2 = 0} = \gamma_3 e^{-\gamma_3 \tau}$, which is a single-exponential decay function with a decay constant γ_3 . Except in all other limiting regimes where the substrate-assisted pathway exists for product desorption, eq S19 will reduces to a single-exponential decay at high substrate concentrations⁵, $f_{on}(\tau) = \gamma_2 e^{-\gamma_2 \tau}$. The high substrate concentrate here derives the product desorption toward the substrate-assisted pathway, making the direct desorption negligible.

Then $\langle \tau_{on} \rangle^{-1}$, which represents the time-averaged product desorption rate for a single nanoparticle, is

$$\langle \tau_{on} \rangle^{-1} = \frac{1}{\int_0^{\infty} \tau f_{on}(\tau) d\tau} = \frac{\gamma_2 a_3 [A][B] + \gamma_3}{1 + a_3 [A][B]} = \frac{\gamma_2 G[B] + \gamma_3}{1 + G[B]} \quad (S20)$$

Here, $a_3 = \gamma_1 / (\gamma_{-1} + \gamma_2)$. The concentration of [A] can be seen as a constant, $G = a_3[A]$.

Consider the limiting conditions for $\langle \tau_{on} \rangle^{-1}$. When $[B] \rightarrow 0$,

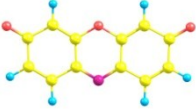

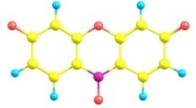

$$\langle \tau_{on} \rangle_{[B] \rightarrow 0}^{-1} = \frac{\gamma_2 G [B] + \gamma_3}{1 + G [B]} = \gamma_3 \quad (\text{S21})$$

When $[B] \rightarrow \infty$,

$$\langle \tau_{on} \rangle_{[B] \rightarrow \infty}^{-1} = \frac{\gamma_2 G [B] + \gamma_3}{1 + G [B]} = \gamma_2 \quad (\text{S22})$$

To give a physical interpretation of [B] dependence of $\langle \tau_{on} \rangle^{-1}$, when $[B] \rightarrow 0$, the forward reaction of reaction 1c is extremely slow ($\gamma_2[B] = 0$), then the product desorption dominantly takes the direct desorption pathway (reaction 1d) and the reaction rate constant is γ_3 . When $[B] \rightarrow \infty$, the product desorption will dominantly take the substrate-assisted pathway (reaction 1c) and the reaction rate constant is γ_2 .

4. Table S1. The planar structure of substrate and product molecules.

| Compound | Top View | Side View |
|---|---|--|
| Resorufin |  |  |
| Resazurin |  |  |
| Note: The atoms with the color of yellow, blue, red and violet represent C, H, O and N, respectively. | | |

5. Conversion of Resazurin to Resorufin at low reactant concentration in the microfluidic cell.

To ensure that the catalytic kinetics of catalyst is not limited by mass transport in our single-molecule image experiments using a flow cell at low reactant concentration,

we should confirm that the supply of the reactants is much larger than their consumption. This confirmation has been done by estimating the consumption and diffusion coefficient,^{3,6} however, experimental data is needed to further confirm that the supply of the reactants is enough. Thus we measured the conversion of Resazurin to Resorufin by fluorescence spectra (Figure S6).

For this goal, firstly, we obtained the fluorescence spectra of Resorufin solutions with known concentrations (three examples shown in Figure S6a, excited with 532-nm green light), and then made a calibration curve between the peak intensity @583nm and the concentration of Resorufin (Figure S6b). Based on the calibration curve obtained here, we can determine the concentrations of Resorufin in the fresh reactant (Inlet) solution and in the outlet solution (Figure S6a), respectively, from the peak intensities of the spectra.

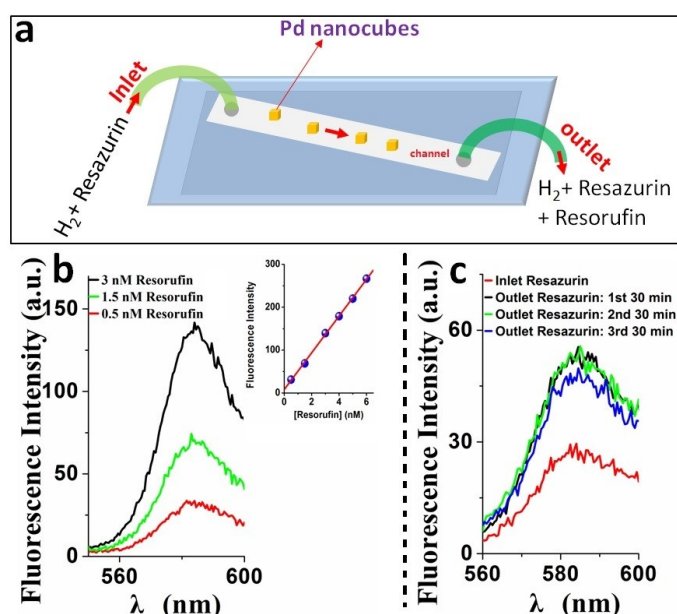


Figure S6. (a) The microflow-cell-based setup for the single-molecule nanocatalysis of individual Pd nanocubes. (b) The measurement of calibration curve between the peak intensity @ 583 nm and the concentrations of Resorufin solutions. (c) Fluorescence spectrum of Resorufin in the fresh reactant and in the outlet solution collected in each 30 min.

In detail, since it has been known that it is always unavoidable for commercial Resazurin to be contaminated by trace amount of Resorufin (*Nano Letters*, 2012, 12, 1253-1259), we then obtained the fluorescence spectrum of fresh reactant (50 nM Resazurin in H₂-saturated solution) excited with green light (532 nm) to determine the concentration of trace Resorufin in fresh commercial Resazurin solution. Indeed, as shown in Figure S6c, the obtained spectrum for fresh inlet solution shows a peak at 583 nm, consistent with that observed on Resorufin solution (Figure S6b). Based on the calibration curve shown in Figure S6b, we found that fresh Resazurin contains

~0.9% Resorufin contamination. After that, under a steady flow rate of 10 $\mu\text{L}/\text{min}$, the reactant solution flowed through a microfluidic cell (Figure S6a) and was then collected from the outlet within the time window of each 30 min, and then their fluorescence spectra were obtained (Figure S6c, black curve: for the first 30 min; green: for the second 30 minutes; blue: for the third 30 minutes).

Based on above analysis, we finally derived that the conversion of Resazurin to Resorufin in the micro-flow cell is about 0.6%, and no obvious deactivation could be observed after long-term (> 1 hour) catalytic reaction (Figure S6c). These results indicate that the consumption of reactant during the catalytic reaction process in the flow cell is very little or negligible due to the very low density of Pd nanoparticles dispersed sparsely on the surface of quartz slide (Figure S6a). As for the concentration of H_2 , since each catalytic cycle consumes one Resazurin (Rin-N-O) molecule and one H_2 molecule: $\text{Rin-N-O} + \text{H}_2 \rightarrow \text{Fin-N} + \text{H}_2\text{O}$, then it can be deduced that the conversion of H_2 in the flow cell is also about 0.6%. Such low conversion rate of the reactant is actually the basis for the assumption made in such type of kinetic analysis that the concentrations of reactants in the cell are constant during the whole reaction process (*Nat. Mater.*, 2008, 7, 992-996; *Angew. Chem. Int. Ed.*, 2010, 49, 8593-8597). This result is also consistent with previous analysis (see SI in *Nat Nanotechnol* 2012,7, 237-241).

6. Distribution of γ_{app} , τ_{off} and τ_{on} of different sizes of Pd nanocubes

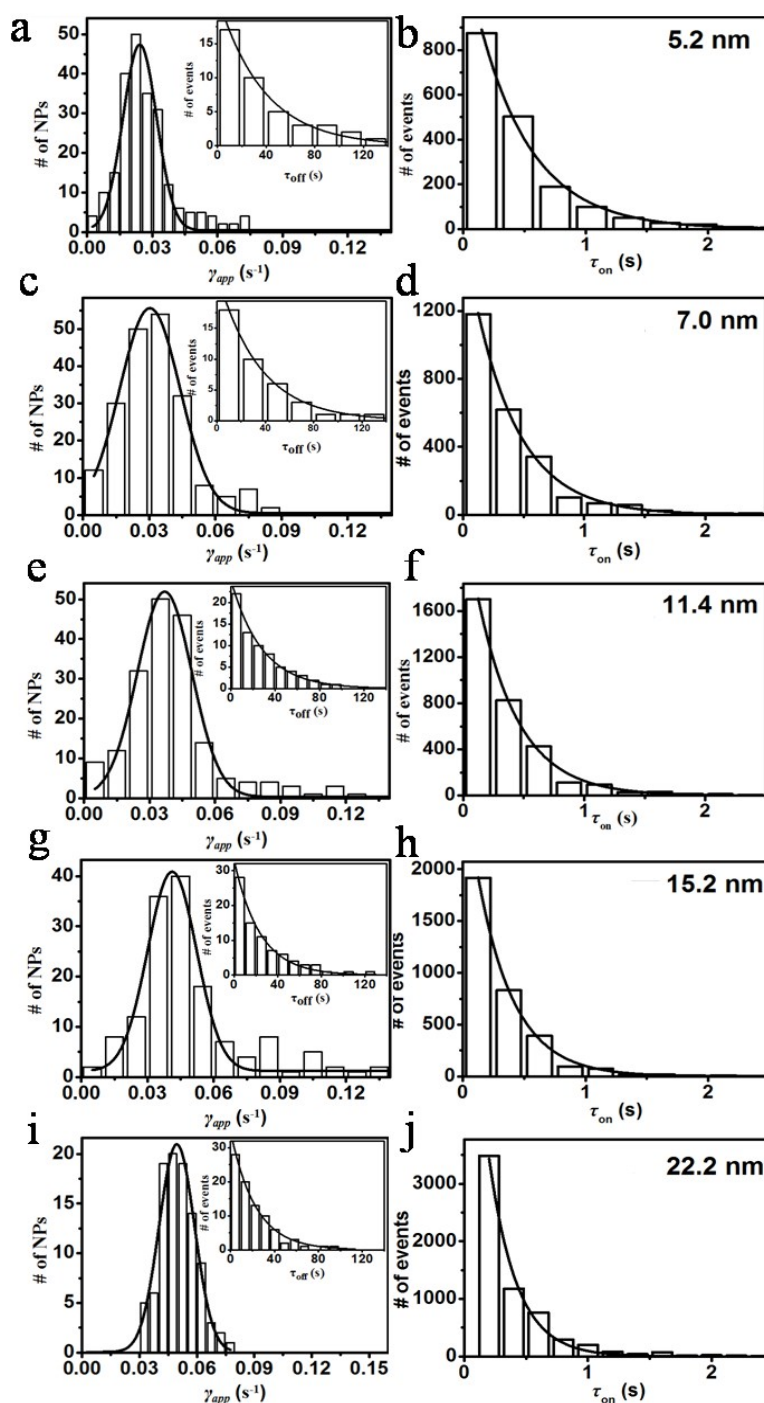


Figure S7. Left: distribution of γ_{app} of (a) 5.2 nm, (c) 7.0 nm, (e) 11.4 nm, (g) 15.2 nm and (i) 22.2 nm nanocubes at 1 nM resazurin; solid lines are Gaussian fits. All experiments are in H₂-saturated solution. Insets: distributions of τ_{off} from a single trajectory; solid line is a single exponential fit with decay constant (a) $\gamma_{app} = 0.026 \pm 0.002$, (c) $\gamma_{app} = 0.029 \pm 0.002$, (e) $\gamma_{app} = 0.036 \pm 0.002$, (g) $\gamma_{app} = 0.042 \pm 0.003$ and (i) $\gamma_{app} = 0.043 \pm 0.003$. Right: distribution of τ_{on} from many trajectories of (b) 5.2 nm, (d) 7.0 nm, (f) 11.4 nm, (h) 15.2 nm and (j) 22.2 nm. Pd nanocubes at 2 nM resazurin; solid lines are single-exponential fits. Other fitting values are listed on Table 2 in main text.

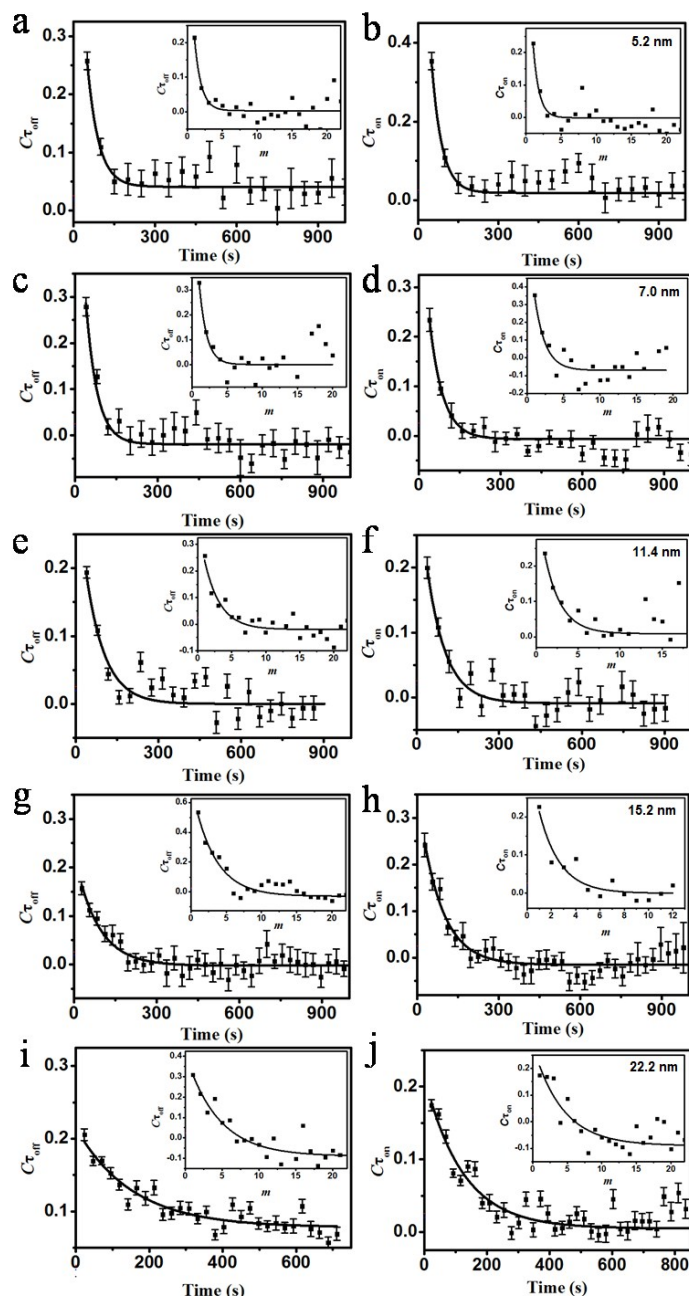


Figure S8. Left: autocorrelation function $C_{\tau_{off}}(t)$ of the microscopic reaction time τ from turnover trajectories of single (a) 5.2 nm, (c) 7.0 nm (e) 11.4 nm, (g) 15.2 nm and (i) 22.2 nm Pd nanocubes at 1nM resazurin and in H_2 -saturated solution. The x -axis was converted from the turnover index m to real time using the average turnover time of each nanoparticle, and each data is an average from >50 trajectories. Solid line is a single exponential fit. Inset: autocorrelation function of the τ_{off} from the turnover trajectory of a single (a) 5.2 nm, (c) 7.0 nm (e) 11.4 nm, (g) 15.2 nm and (i) 22.2 nm Pd-nanocube; solid line is a single exponential fit with decay constant of (a) 0.8 ± 0.3 , (c) 1.1 ± 0.5 , (e) 2.3 ± 0.6 , (g) 3.2 ± 0.4 and (i) 4.5 ± 1.1 turnovers. Right: same for the upper but for the τ_{off} reaction at 1 nM resazurin of (b) 5.2 nm, (d) 7.0 nm, (f) 11.4 nm, (g) 15.2 nm and (i) 22.2 nm Pd nanocubes. Data is an average from >50 trajectories. Inset: same as upper inset and the decay constant is (b) 1.0 ± 0.3 , (d) 1.5 ± 0.6 , (f) 2.0 ± 1.0 , (h) 2.2 ± 0.4 and (j) 4.3 ± 1.3 turnovers. Other fitting values are listed on Table 2 in main text.

- (1) Han, K. S.; Liu, G.; Zhou, X.; Medina, R. E.; Chen, P. *Nano Lett.* **2012**, *12*, 1253.
- (2) Xu, W.; Kong, J. S.; Yeh, Y.-T. E.; Chen, P. *Nat. Mater.* **2008**, *7*, 992.
- (3) Xu, W.; Shen, H.; Kim, Y. J.; Zhou, X.; Liu, G.; Park, J.; Chen, P. *Nano letters* **2009**, *9*, 3968.
- (4) Xu, W.; Kong, J. S.; Chen, P. *J. Phy. Chem. C* **2009**, *113*, 2393.
- (5) Xu, W.; Kong, J. S.; Chen, P. *Phy. Chem. Chem. Phy.* **2009**, *11*, 2767.
- (6) Zhou, X.; Andoy, N. M.; Liu, G.; Choudhary, E.; Han, K.-S.; Shen, H.; Chen, P. *Nat Nano* **2012**, *7*, 237.